Biomedicine & Pharmacotherapy 187 (2025) 118083

Contents lists available at ScienceDirect

Biomedicine & Pharmacotherapy

journal homepage: www.elsevier.com/locate/biopha

RvD1 and LXA_4 inhibitory effects on cardiac voltage-gated potassium channels

Alicia De la Cruz [a,b,*], Carlotta Ronchi [c], Chiara Bartolucci [d], Paula G. Socuéllamos [a,1], Angela de Benito-Bueno [a], Stefano Severi [d], Antonio Zaza [c], Carmen Valenzuela [a,e,**]

[a] Instituto de Investigaciones Biomédicas Sols-Morreale CSIC-UAM, Madrid, Spain
[b] Department of Biomedical and Clinical Sciences, Linköping University, Linköping, Sweden
[c] Department of Biotechnology and Biosciences, Università degli Studi di Milano-Bicocca, Milan, Italy
[d] Department of Electrical, Electronic and Information Engineering 'Guglielmo Marconi', University of Bologna, Cesena, Italy
[e] Network of Cardiovascular Diseases (CIBERCV), Spain

ARTICLE INFO

Keywords:
RvD1
LXA_4
I_{Ks}
$K_V7.1$
KCNE1
$K_V11.1$

ABSTRACT

The resolution of inflammation is modulated by specialized pro-resolving lipid mediators (SPMs), which can be modified in some cardiovascular diseases. Among these SPMs, RvD1 and LXA_4 prevent atrial fibrillation (AF) remodeling and cardiac hypertrophy, respectively in animal models. However, little is known about their electrophysiological effects on cardiac voltage-gated (VG) ion channels. We used the patch-clamp technique in heterologous systems and cardiomyocytes to assess the acute effects of RvD1, and LXA_4, on VG potassium currents. *In silico* simulations were used to predict the effect of current modulation on the atrial and ventricular action potentials (AP). RvD1 (5 nM) reduced I_{Ks} (channel $K_V7.1$/KCNE1) in COS-7 cells and guinea-pig cardiomyocytes by 50.3 ± 7.3 % and 29.9 ± 5.4 % at + 40 mV, respectively, without modifying its voltage dependence. RvD1 was more potent than LXA_4. In heterologous systems, RvD1 was also tested on I_{Kur} (channel $K_V1.5$), I_{to} (channel $K_V4.3$/KChIP2), I_{Kr} (channel $K_V11.1$), and I_{K1} (channel $K_{ir}2.1$) with the largest inhibitory effect on I_{Ks} and I_{Kr}. In *in silico* simulations RvD1 prolonged repolarization significantly in both atrial and ventricular myocytes. All these results provide a comprehensive evaluation of RvD1 and LXA_4 on cardiac human potassium channels, at pathophysiologically relevant concentrations, being RvD1 more potent than LXA_4. The predicted effects on the AP suggest that, along with their antiinflammatory action, RvD1 may reverse AF-induced electrical remodeling in the atria by their modulation of K^+ currents. The same action might instead contribute to ventricular functional remodeling; however, direct evidence for this is missing.

1. Introduction

Derivatives of n-3 and n-6 polyunsaturated fatty acids (PUFAs), collectively named SPMs, include several members grouped into 4 families: lipoxins, protectins, maresins, and resolvins [1–4]. Among SPMs, resolvins (RvDs) may be endowed with important cardiac antiarrhythmic effects; indeed, RvD1 prevented AF and countered atrial pro-arrhythmic remodeling in experimental models [5,6]. Also, RvD1 attenuated pressure overload-induced cardiac hypertrophy [7], protects the heart against LPS-induced injuries [8] and also from cardiac toxicity induced by doxorubicin [9].

Inflammation strongly contributes to the progression of cardiovascular disease observed in atrial fibrillation [6] and RvD1 is endowed with a potent anti-inflammatory and pro-resolution effectiveness [10–13]. Moreover, RvD2 protected cardiovascular function and structure, by modulating vascular factors, fibrosis, and inflammation, when administered before and after the development of hypertension [14]. Therefore, SPMs antiarrhythmic effects have been so far attributed to

* Corresponding author at: Department of Biomedical and Clinical Sciences, Linköping University, Linköping, Sweden.
** Correspondence to: Instituto de Investigaciones Biomédicas Sols-Morreale CSIC-UAM, C/Arturo Duperier 4, Madrid 28029, Spain.
E-mail addresses: alicia.de.la.cruz.fernandez@liu.se (A.D. Cruz), carlottaronchi.phd@gmail.com (C. Ronchi), chiara.bartolucci4@unibo.it (C. Bartolucci), paula.garcia@cnic.es (P.G. Socuéllamos), angela.db.94@gmail.com (A. Benito-Bueno), stefano.severi@unibo.it (S. Severi), antonio.zaza@unimib.it (A. Zaza), cvalenzuela@iib.uam.es (C. Valenzuela).
[1] present address: Centro Nacional de Investigaciones Cardiovasculares (CNIC, Madrid, Spain)

https://doi.org/10.1016/j.biopha.2025.118083
Received 9 January 2025; Received in revised form 11 April 2025; Accepted 21 April 2025
Available online 23 April 2025

their role in the resolution of inflammation. It has been described that SPMs modulate different ion channels [15–17]. Nontheless, the effects of PUFAs (SPMs precursors) directly modulate voltage-gated (VG) ion channels (Na_V, Ca_V and K_V) to the extent that they have been proposed as potential anti-arrhythmic drugs [18–25]. Therefore, regulation of VG ion channels by SPMs, thus far poorly investigated, might be relevant to cardiac electrophysiology.

In the present study we have analyzed the effects of resolvins (RvD1), and lipoxins (LXA_4) on a variety of VG K^+ channels, an information relevant to the pathogenesis of arrhythmias and evolution of cardiac diseases, whether including inflammation or not. Our results show that RvD1 and LXA_4 inhibited $K_V7.1$/KCNE1 and $K_V11.1$ channels, with minor changes in their voltage dependence, being RvD1 more effective than LXA_4. $K_V1.5$, $K_{ir}2.1$, and $K_V4.3$/KChIP2 channels were affected by SPMs to a lesser extent.

2. Materials and methods

2.1. Experimental models

2.1.1. Primary cells. Guinea-pig cardiac ventricular myocytes

All animal care and experimental procedures were performed conforming to the NIH guidelines (Guide for the care and use of laboratory animals) revised in 2011; and from Directive 2010/63/EU of the European Parliament on the protection of animals used for scientific purposes and approved by the University of Milano-Bicocca ethics review board.

Adult Dunkin-Hartley Guinea-Pig (body weight 300 g, Envigo) were anesthetized with Ketamine + Xylazine (130 +7.5 mg/Kg) i.p. and euthanized by cervical dislocation.

2.1.2. Isolation of cardiomyocytes, culture of cell lines and transfection

Ventricular cardiomyocytes were isolated by using a previously published [26] retrograde aortic perfusion method with minor modifications. After isolation, the medium Ca^{2+} concentration was gradually restored to 1 mM and the cells were stored at + 4°C until use. Only rod-shaped, Ca^{2+}- tolerant cardiomyocytes were used within 12 h from dissociation. Electrophysiological measurements in guinea-pig ventricular cardiomyocytes were performed with the whole-cell patch-clamp configuration.

COS-7, *Ltk*$^-$ and CHO-K1 cells were cultured in DMEM (COS-7 and *Ltk*$^-$) or Iscove's modified Eagle's (CHO-K1) supplemented with 10 % (v/v) FBS, and 100 IU/ml of penicillin and 100 μg/ml streptomycin (all from Gibco) [20,27]. CHO-K1 cells medium was supplemented with 1 % (v/v) L-Glutamine; and *Ltk*$^-$ cells medium was supplemented with 0.25 mg/ml G418. Cells were cultured in an atmosphere with 5 % CO_2 at 37°C. COS-7 cells have an endogenous acid-sensitive potassium current [28], which did not interfere with the recordings obtained after transfecting the cells with K_V7 or K_V1 subfamilies channels nor with $K_{ir}2.1$, which were the potassium channels of interest to us.

For electrophysiological recordings, COS-7 cells were incubated in 35 mm pretreated sterilized culture dishes (Falcon) and transiently transfected with 0.5 μg pEYFP-N1-KCNQ1 or co-transfected with 0.5 μg pEYFP-N1-KCNQ1 and 0.5 μg pECFP-C1-KCNE1. To record I_{K1}, 0.5 μg of $K_{ir}2.1$ cloned into pcDNA3.1 (gift from Dr. E. Delpón, Universidad Complutense de Madrid, Spain) was transfected in COS-7 cells for electrophysiological recordings. $K_V11.1$ recordings were carried out in COS-7 cells after transfection with 1 μg of $K_V11.1$ (cloned into a pcDNA3.1, kindly provided by Drs. S. Nattel, T. E. Hébert, and W. Weerapura). Stably transfected *Ltk*$^-$ cell line with the gene encoding $K_V1.5$ channel was a gift of Dr. M.M. Tamkun (Colorado State University, USA) [29]. Before use, subconfluent cultures were incubated with 2 μM dexamethasone (D4902, Sigma-Aldrich, Saint Louis, MO, USA) for 24 h. CHO-K1 cells were transiently co-transfected with 2 μg $K_V4.3$ (cloned into pBK-CMV vector, amplified by PCR and ligated into pmCherry-C1 (Clontech), by using *XhoI* and *HindIII* restriction sites [30], and 1 μg KChIP2 (cloned into IRES mCherry KChIP2 using *XbaI* and *XhoI* restriction sites).

In all cases, the cDNA was transient transfected together with 0.5 μg of the reporter plasmid EBO-pcD-Leu2-CD8 (to select transfected cells) per 35 mm culture dish [31] in cells at 60–80 % confluence following the FuGENE6 transfection method (Promega). The ratio μg DNA:μl Fugene was 1:3. Before use, cells (COS-7 and CHO-K1 cells) were incubated with polystyrene microbeads precoated with anti-CD8 antibody (Dynabeads M450, Dynal) and were removed from culture plates using TrypLE™ Express (Life Technologies) [20,32].

2.2. Electrophysiological recordings

Guinea-pig ventricular cardiomyocytes were superfused through a thermostated pipette; the solution temperature was also monitored at the pipette tip with a fast-response digital thermometer (BAT-12, Physitemp, Clifton, NJ, USA) and kept at 36 ± 0.5°C. The extracellular (bath) solution contained (in mM): 154 NaCl, 4 KCl, 2 $CaCl_2$, 1.2 $MgCl_2$, 5 HEPES-NaOH, and 5.5 glucose (pH=7.4 with KOH); and intracellular (pipette-filing) solution contained (in mM): 110 K-aspartate, 23 KCl, 2 $CaCl_2$, 5 phosphocreatine, 3 $MgCl_2$, 0.4 Na-GTP, 5 Na-ATP, 5 HEPES-K, and 5 EGTA-K (pH=7.3 with KOH). Membrane capacitance and series resistance were measured in every cell. Signals were filtered at 0.4 kHz (Axon Multiclamp 700B, Molecular Devices, Sunnydale, CA, USA), and digitized through a 12-bit A/D converter (Axon Digidata 1440 A, Molecular Devices, Sunnydale, CA, USA) with a sampling rate of 1 kHz. The slow delayed rectifier potassium current (I_{Ks}) was isolated as the current sensitive to 2 μM JNJ303 (Tocris). 10 μM nifedipine 5 μM E4031 and 1 μM SEA0400 (all from Sigma-Aldrich) were added to Tyrode's solution to minimize contamination by the L-type Ca channel (I_{CaL}), the rapid delayed rectifier potassium current (I_{Kr}), and the Na^+/Ca^{2+} exchanger current respectively. The Na^+ current was inactivated by setting the holding potential at −40 mV. I_{Ks} was activated by 5 s V-steps from a holding potential of −40 mV. In Protocol 1 I_{Ks} was measured at a single potential (+40 mV) before and after steady-state drug application within the same myocyte (internal control); in Protocol 2, complete I_{Ks} current-voltage (I-V) relationships were obtained in separate cell groups previously incubated with control and SPMs-containing solutions respectively. I_{Ks} amplitude was measured at the end of the activating step (end-step current) and immediately after the return to the holding potential (tail current). To obtain the activation curves, tail current amplitudes were normalized to the maximal one. Summarizing, in Protocol 1, I_{Ks} was elicited by applying a single potential (+40 mV) from a holding potential of −40 mV. Tail currents were recorded at −40 mV. In Protocol 2, complete I_{Ks} current-voltage (I-V) relationships were obtained after applying 5 s pulses from a holding potential of −40 mV to + 60 mV in 20-mV steps, followed by a repolarizing pulse to −40 mV to record the tail currents.

For measurements of the activity of potassium channels in transfected cell lines (COS-7, CHO-K1 and *Ltk*$^-$ cells), the external solution contained (in mM): 130 NaCl, 4 KCl, 1.8 $CaCl_2$, 1 $MgCl_2$, 10 HEPES-Na, and 10 glucose (pH=7.4 with NaOH). Internal pipette-filing solution contained (in mM): 80 K-aspartate, 50 KCl, 3 phosphocreatine, 10 KH_2PO_4, 3 Mg-ATP, 10 HEPES-K, and 5 EGTA-K (pH=7.25 with KOH). I_{Kur} (channel $K_V1.5$), I_{to} (channel $K_V4.3$/KChIP2), I_{Kr} (channel $K_V11.1$), and I_{K1} (channel $K_{ir}2.1$) were recorded in the whole-cell configuration as previously reported [16,27,32,33] at room temperature (23–25°C). I_{Ks} (from $K_V7.1$ channels alone, or coexpressed with KCNE1) was recorded in the perforated patch-clamp configuration (Amphotericin-B, disolved in DMSO, was added to the pipette solution to achieve a final concentration of 100 μg/ml) [20]. I-V relationships were constructed by measuring the currents at the end of the activating step [20,34].

Micropipettes were pulled from borosilicate glass capillary tubes (GD-1 model, Narishige, London, UK) on a horizontal puller (P-87, Sutter Instrument Co., CA, USA) and heat-polished with a microforge (MF-83, Narishige). After heat-polishing, the resistance of the patch electrodes tip (filled with the internal solution) averaged 2–4 MΩ [20].

GΩ seal formation was achieved by suction; thereafter, capacitance and series resistance were compensated by about 80 %. As a result, uncompensated series resistances were in the 4–8 MΩ range, thus, biasing voltage by less than 2 mV.

Signals were amplified by Axopatch-200B (Molecular Devices, Sunnydale, CA, USA), lowpass filtered (1 kHz) and sampled at 2 kHz (I_{Ks}) or 4 kHz (other currents) by the A/D converter Digidata 1440 A (Molecular Devices). Signals were further filtered (4-pole Bessel filter) at 1 kHz (I_{Ks}) or 2 kHz (other currents). Command voltages and data acquisition were controlled with pClamp11 software (Molecular Devices).

The holding potential was set to −80 mV (unless otherwise indicated), and the interpulse interval was set to 10 s (for K_V1.5, K_V4.3/KChIP2, Kir2.1) or 30 s (for K_V7.1/KCNE1 and K_V11.1). The voltage pulse protocols were designed to analyze the biophysical properties of each channel and are shown in Figures. Briefly, for K_V7.1/KCNE1, I-V protocol were obtained after applying 5.5 s pulses from a holding potential of −80 mV to + 100 mV in 20-mV steps, followed by a repolarizing pulse to −40 mV to record the tail currents. For K_V11.1, I-V protocol were obtained after applying 5 s pulses from a holding potential of −80 mV to + 50 mV in 10-mV steps, and followed by a repolarizing pulse to −60 mV to record the tail currents. K_V1.5, K_V4.3/KChIP2 elicited currents were obtained after applying 250-ms depolarizing pulses from −80 mV to + 60 mV in 10 mV steps, but for K_V4.3/KChIP2 elicited currents, a −100 mV pre-pulse was applied. K_{ir}2.1 elicited currents were obtained after applying 500-ms depolarizing pulses from −140 mV to 0 mV in 10-mV steps.

Time constants of current activation, inactivation, and deactivation were determined by fitting the recordings with mono- or bi-exponential functions:

$$y = A_1 \exp(-t/\tau_1) + A_2 \exp(-t/\tau_2) + C$$

where τ_1 and τ_2 are time constants, A_1 and A_2 are the amplitudes of each component of the exponential, and C is the baseline value [35,36]. The voltage dependence of channel activation was fitted to a Boltzmann equation:

$$y = 1/[1 + exp(-(E - V_{1/2})/s)]$$

in which *s* represents the slope factor, E represents the applied voltage, and $V_{1/2}$ the voltage at which 50 % of the channels are activated [31,35]. Origin 2020b (OriginLab Software, Northampton, MA, USA) and CLAMPFIT 10.6 software from the PCLAMP 10 package were used to analyze data, perform least-squares fitting and for data presentation.

2.3. In-silico action potential analysis

To predict the effects of the SPMs (RvD1, and LXA_4) on the action potential (AP), two human ventricular models, the Bartolucci-Passini-Severi (BPS) [37] and the gold standard model O'Hara–Rudy (ORd) [38], and two human atrial models,Mazhar-Bartolucci-Severi (MBS) and the Koivumaki (K) [39,40] were used. These models have been widely validated against experimental data, including human electrophysiological recordings and AP characteristics, ensuring their reliability in simulating cardiac electrical activity in each related publication [37–40]. The ORd model is widely recognized for its detailed representation of human ventricular electrophysiology and has been validated against experimental data from isolated human ventricular myocytes. It accounts for ion channel kinetics, intracellular calcium cycling, and dynamic changes in ionic concentrations, making it suitable for simulating drug effects. The BPS model is a modified version of the ORd ventricular model, incorporating additional refinements in ionic current formulations to improve accuracy in $[Ca^{2+}]_o$-APD (Action potential duration) dependency and in simulating cardiac abnormalities, such as EADs (early afterdepolarizations), DADs (delayed afterdepolarizations) and alternans. For atrial simulations, the K model is a biophysically detailed representation of human atrial electrophysiology that includes descriptions of key atrial ion channels, calcium handling, and AP variability under different pacing rates. The MBS model, a more recent human atrial model, integrates updated formulations for key ionic currents and has been specifically optimized to reproduce atrial APD characteristics and a plethora of human atrial experimental data. For ventricular simulations, models for isolated endocardial, epicardial, and M myocytes were used. To simulate RvD1 (at 5 and 50 nM), and LXA_4 effects, the models were parametrized according to the experimental results reported in Table 1, assuming that the data obtained in the heterologous system can be preserved in a cardiomyocyte. The effect on activation V-dependency was simulated by changing the original $V_{1/2}$ parameter by the compound-induced shift (e.g. under RvD1 at 5 nM, for I_{Ks} the shift was 4.1 mV, see Table 1) and the slope factor by the % compound-induced change. Simulations were carried out by considering SPMs effect on a single current at a time or by incorporating all the affected currents. All models were paced at the basic cycle length of 1000 ms to steady state (> 1000 cycles). The action potential duration was measured at 90 % repolarization (APD_{90}). Model equations were implemented in Matlab 2021b (The MathWorks Inc., Natick, MA, USA) and numerically solved using the ode15s solver.

2.4. Drugs and reagents

(S)-Resolvin D1 (or RvD1) (Cayman Chemical, Ann Arbor, MI, USA), and LXA_4 (Santa Cruz Biotechnology, Dallas, USA) were dissolved in ethanol (final concentration 1 μM) and stored protected from light at −80ºC. For electrophysiological recordings, each SPM was dissolved in the extracellular solution at concentrations in the 5–500 nM range. This SPMs concentrations were selected since different studies have reported that the serum levels of RvD1 and LXA_4 in control human beings are in between 0.4 and 18 nM. Lower levels are found in patients suffering pathologies involving chronic inflammation, such as atrial fibrillation, hypertension, myocardial infarction or aneurysmal subarachnoid hemorrhage [7,41–43]. Control solution contained the same percentage of ethanol than the extracellular solution containing the SPMs.

2.5. Statistical analysis

Data are expressed as mean ± SEM of n measurements. Comparisons between mean values were performed by using the Student's *t*-test or ANOVA, as appropriate (Bonferoni's correction in post–hoc comparisons). Statistical significance was defined as $P < 0.05$. Sample size (n) is reported in figure legends.

3. Results

3.1. RvD1 and LXA_4 effects on K_V7.1/KCNE1 in COS-7 cells

Fig. 1A shows I_{Ks} (K_V7.1/KCNE1) recordings obtained in the absence and the presence of RvD1. I-V protocol were obtained after applying 5 s pulses from a holding potential of −80 mV to + 100 mV in 20-mV steps, and followed by a repolarizing pulse to −40 mV to record the tail currents. RvD1 5 and 50 nM inhibited I_{Ks} amplitude by 48.6 ± 5.7 % (n = 5, $P < 0.01$) and 86.3 ± 5.0 % (n = 6, $P < 0.01$) respectively, measured at the end of 5.5 s pulses at + 60 mV.

Fig. 1B shows the RvD1 (5 and 50 nM) effect on I_{Ks} I-V relationship. At both concentrations, RvD1 inhibited I_{Ks} at membrane potentials positive to 0 mV. Neither the activation $V_{1/2}$ nor the slope factor were modified (Table 1). RvD1 effects were neither voltage-dependent, (Fig. 1D), nor time-dependent (Tables 2 and 3). I_{Ks} inhibition by RvD1 was largely reversible upon wash-out (73.5 ± 17.8 %, n = 4 vs. control conditions, $P > 0.05$, Fig. 1E).

RvD1 (5 and 50 nM) effects on K_V7.1 in the absence of KCNE1 were also studied (Figure S1). At 5 nM, RvD1-induced block was weaker than that observed with this compound on K_V7.1/KCNE1 (28.9 ± 5.8 % n = 5, $P < 0.05$, measured at the end of 5.5 s pulses at +60 mV).

Table 1
Effects of SPMs on the voltage dependence on K_V7.1/KCNE1, K_V7.1, K_V1.5 and K_V4.3/KChIP2 and K_V11.1.

	K_V7.1/KCNE1		K_V7.1		K_V1.5		K_V4.3/KChIP2		K_V11.1	
	$V_{1/2}$ (mV)	s (mV)	$V_{1/2}$ (mV)	s (mV)	$V_{1/2}$ (mV)	s (mV)	$V_{1/2}$ (mV)	s (mV)	$V_{1/2}$ (mV)	s (mV)
Control	34.5 ± 4.9	20.2 ± 1.8	−16.5 ± 2.3	7.1 ± 0.8	−12.9 ± 1.0	5.7 ± 0.4	26.3 ± 2.4	15.4 ± 1.1	−6.6 ± 2.3	8.3 ± 0.4
RvD1 (5 nM)	35.6 ± 11.1	18.0 ± 1.6	−11.6 ± 1.8 *	8.9 ± 0.7	−14.3 ± 1.3	6.1 ± 0.4	34.0 ± 1.9 *	17.4 ± 0.5	−7.5 ± 4.5	8.5 ± 0.4
Control					−11.5 ± 1.4	5.6 ± 0.4	26.3 ± 2.4	15.4 ± 1.1	−6.5 ± 3.8	8.6 ± 0.5
RvD1 (50 nM)					−10.0 ± 2.3	5.1 ± 0.6	29.7 ± 2.3 *	16.4 ± 1.0	−2.7 ± 4.5 *	7.0 ± 0.9
Control	48.5 ± 2.4	21.8 ± 2.2								
LXA_4 (500 nM)	42.0 ± 4.1	21.7 ± 1.3								

Data are shown as the mean ± SEM. *: $P < 0.05$ (Paired Student's *t*-test), n = 4–8.

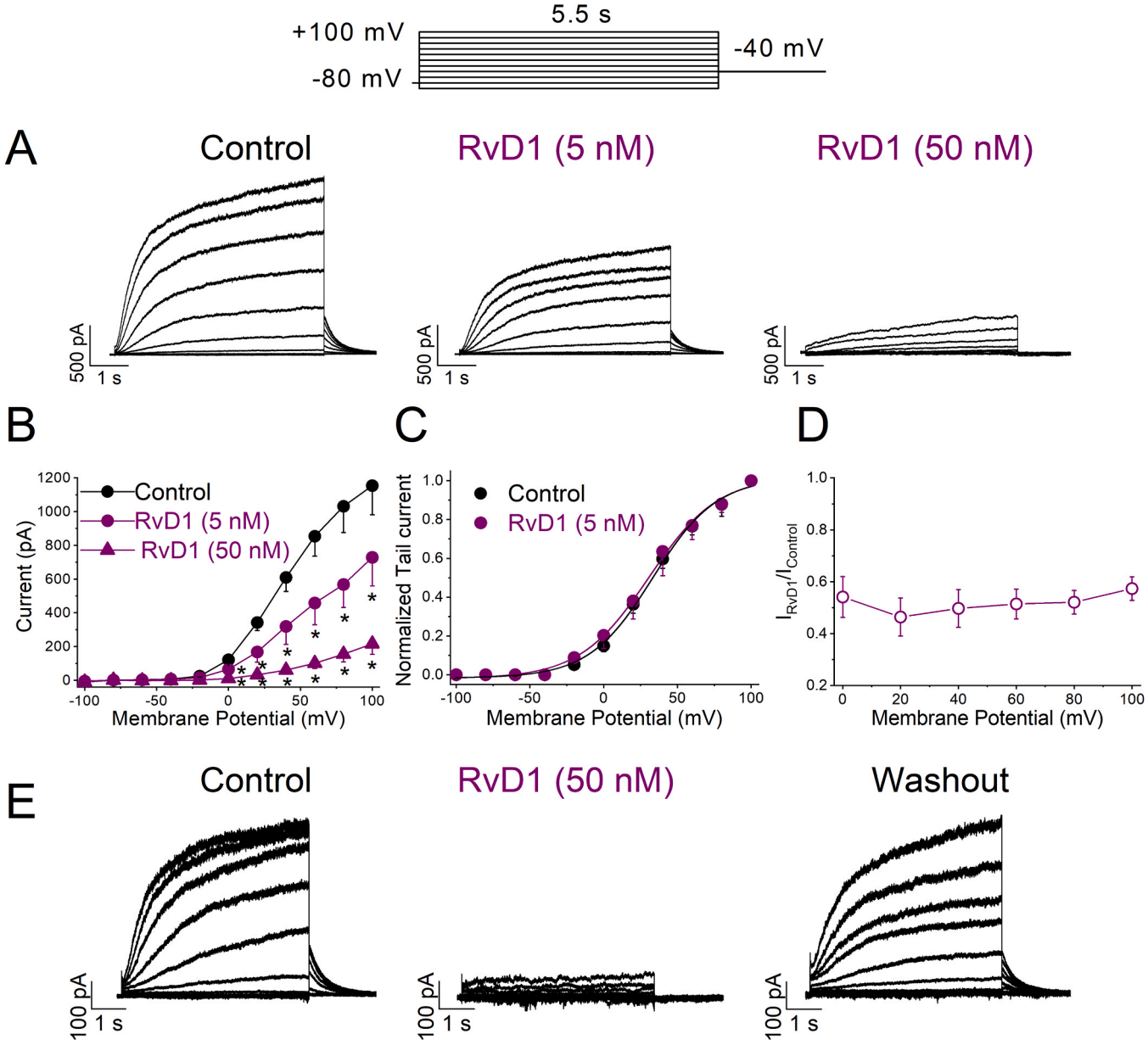

Fig. 1. Voltage-dependent effects of RvD1 on K_V7.1/KCNE1 (I_{Ks}) in transiently transfected COS-7 cells. A: Current traces in the absence and in the presence of 5 and 50 nM RvD1. B: I-V relationships obtained after plotting the current at the end of 5.5-s vs. membrane potential, in the absence and in the presence of RvD1. C: Activation curves of I_{Ks} in the absence and in the presence of 5 nM RvD1. D: Ratio between the current in the presence of 5 nM RvD1 and under control conditions. E: Representative traces of 50 nM RvD1 wash-out on I_{Ks}. Data are shown as the mean ± SEM. *$P < 0.05$ (Paired Student's *t*-test), n = 5–8.

Table 2
Activation Kinetics.

$K_V7.1$/KCNE1				
Control		RvD1 (5 nM)		
τ_s (ms)	τ_f (ms)	τ_s (ms)	τ_f (ms)	(n, P)
3608.3 ± 981.4	908.5 ± 197.1	3577.5 ± 784.1	920.2 ± 181.4	n = 6, P > 0.05
Control		*LXA_4 (500 nM)*		
τ_s (ms)	τ_f (ms)	τ_s (ms)	τ_f (ms)	
3340.0 ± 851.7	726.5 ± 160.4	2506.7 ± 369.8	674.5 ± 194.4	n = 7, P > 0.05
$K_V7.1$				
Control		*RvD1 (5 nM)*		
τ (ms)		τ (ms)		
16.0 ± 4.5		34.7 ± 9.2		n = 3, P > 0.05

Data are shown as the mean ± SEM. * : $P < 0.05$ (Paired Student's *t*-test), n = 3–7.

Table 3
Deactivation kinetics.

$K_V7.1$/KCNE1		
Control τ (ms)	RvD1 (5 nM) τ (ms)	(n, P)
426.1 ± 95.3	464.6 ± 90.6	n = 5, P > 0.05
Control *τ (ms)*	LXA_4 (500 nM) τ (ms)	
357.9 ± 50.1	429.6 ± 41.7 *	n = 7, P < 0.05
$K_V7.1$		
Control τ (ms)	RvD1 (5 nM) τ (ms)	
303.0 ± 52.8	375.4 ± 92.3	n = 3, P > 0.05

Data are shown as the mean ± SEM. * : P < 0.05 (Paired Student's *t*-test), n = 3–7.

However, in this case, RvD1 shifted the activation $V_{1/2}$, by + 5 mV without modifying the slope factor (Table 1) and activation kinetics (Tables 2 and 3). These results suggest that KCNE1 tunes the sensitivity of $K_V7.1$ to RvD1, being RvD1 more potent to block these channels in the presence of this β-subunit (Fig. 1 and S1).

Fig. 2 shows the effects of 500 nM LXA_4 on I_{Ks}. LXA_4 inhibited I_{Ks} by 33.0 ± 3.4 % (n = 5, $P < 0.01$) measured at the end of 5.5 s pulses at + 60 mV, (Fig. 2A). As shown by the I-V relationship (Fig. 2B), LXA_4 decreased the current magnitude at membrane potentials positive to 0 mV.

LXA_4 modified neither the $V_{1/2}$ nor the slope of the I_{Ks} activation curve (Fig. 2C and Table 1). LXA_4-induced block was not voltage-dependent, being similar at + 20 mV and + 100 mV (Fig. 2D) and did not affect activation kinetics (Table 2). However, LXA_4 slowed the deactivation process (Table 3). LXA_4 effects were almost completely reversible on wash-out (89.3 ± 4.5 %, n = 6, P > 0.05 vs. control conditions, Fig. 2E). Overall, albeit qualitatively similar to that of RvD1, LXA_4 effects on I_{Ks} was quantitatively smaller. Both agents failed to modify current kinetics and their effct was largely reversible.

3.2. RvD1 and LXA_4 effects on I_{Ks} of guinea-pig ventricular cardiomyocytes

When using the internal control (Protocol 1) (Figs. S2C), 5 nM RvD1 inhibited I_{Ks} measured at the end step by 29.9 ± 5.4 % at + 40 mV (n ≥ 6, $P < 0.05$), the effect with 50 nM RvD1 was similar (28.1 ± 4.3 %, n ≥ 6, $P < 0.05$). At the same potential, LXA_4 (500 nM) inhibited the end-step of the I_{Ks} by 56.0 ± 6.0 % and the tail current by 45.2 ± 6.0 % (n = 8, $P < 0.05$) (Figure S3B).

RvD1 and LXA_4 effect on the I_{Ks} I-V relationship was tested by comparing separate cell groups incubated with the control and test solutions respectively (Protocol 2). Fig. 3A shows representative recordings from three groups of cardiomyocytes in control conditions (black), after incubation with 5 nM RvD1 (red) and 50 nM RvD1 (blue) respectively. RvD1 5 nM significantly inhibited the end-step and tail currents (Fig. 3B-C) at all potentials (n ≥ 10, $P < 0.05$); the step/tail ratio (at +60 mV) was unchanged (3.64 ± 0.57 vs 2.8 ± 0.16; NS). RvD 50 nM did not further reduce current amplitude, but significantly increased the step/tail raio (3.84 ± 0.35 vs 2.8 ± 0.16; $P < 0.05$), thus indicating an effect inversely proportional to the current driving force. Fig. 3D shows that RvD1 (5 and 50 nM) did not modify the $V_{1/2}$ or the slope factor of the activation curve ($V_{1/2}$: Control 21.7 ± 2.4 mV; RvD1 (5 nM) 17.4 ± 2.4 mV; RvD1 (50 nM) 25.6 ± 1.6 mV; Slope: Control 11.2 ± 0.95 mV; RvD1 (5 nM) 8.54 ± 1.1 mV; RvD1 (50 nM) 10.0 ± 1.8 mV).

Fig. 4A shows representative I_{Ks} recordings from two groups of cardiomyocytes in control condition (black) and after incubation with control LXA_4 (light blue). LXA_4 inhibited the end-step and tail currents (Fig. 4B-C) at all potentials, (n ≥ 10, $P < 0.05$); the step/tail ratio (at +60 mV) was unchanged (2.91 ± 0.57 vs 2.8 ± 0.16; NS). Fig. 4D shows that LXA_4 did not modify the I_{Ks} activation curve ($V_{1/2}$ = 21.7 ± 2.4 mV vs. 15.7 ± 2.6, in control and LXA_4, respectively; Slope = 11.2 ± 0.95 mV vs. 9.5 ± 1.4 mV, in control and LXA_4, respectively; n = 15 and n = 8, in control and LXA_4, respectively, $P > 0.05$).

3.3. RvD1 effects on other cardiac voltage-gated potassium channels

Next, we wanted to elucidate whether RvD1 also inhibits other cardiac potassium channels. To this aim, we studied the effects of RvD1 in heterologous systems (COS-7, CHO-K1 and *Ltk*$^-$ cells) transfected with different cardiac potassium channels.

3.3.1. RvD1 effects on $K_V1.5$ (in *Ltk*$^-$ cells)

$K_V1.5$ channels carry an ultra-rapid delayed rectifier potassium current (I_{Kur}), which plays an essential role in phases 1 and 2 of atrial repolarization. Fig. 5A-B show I_{Kur} and its I-V relationship. RvD1 (5 nM) slightly inhibited I_{Kur} (at the end of the activating step) at all potentials (at +60 mV 6.9 ± 1.0 %; n = 8, $P < 0.01$); and at 50 nM had a somewhat larger effect (28.2 ± 2.5 %; n = 7, $P < 0.05$) measured at the end of 250 ms at the same potential. The activation curve and the slope factor were not modified at either of the two concentrations tested (Table 1, Fig. 5C). RvD1-induced block was not voltage-dependent (Data not shown).

3.3.2. RvD1 effects on $K_V4.3$/KChIP2 (in CHO cells)

The $K_V4.3$/KChIP2 complex carries the main component of I_{to}, the fast repolarizing current responsible for phase 1 of the AP, particularly prominent in atrial myocytes. Fig. 5D-E shows that RvD1 5 nM moderately inhibited I_{to} (17.5 ± 2.2 % at +60 mV; n = 4, $P > 0.05$) at all potentials; RvD1 50 nM had a somewhat stronger effect (27.3 ± 2.0 %; n = 4, $P > 0.05$). The activation $V_{1/2}$ and the slope factor were not modified by 5 nM RvD1; and RvD1 50 nM slightly shifted $V_{1/2}$ towards more positive potentials (Table 1, Fig. 5F). Block produced by RvD1 was not voltage-dependent (Data not shown).

3.3.3. RvD1 effects on $K_V11.1$ (hERG) (COS-7 cells)

$K_V11.1$ (hERG) channels carry I_{Kr}, a major contributor to repolarization particularly in ventricular myocytres. I_{Kr} inactivates with membrane depolarization; thus, at positive step potentials, the current may be larger upon repolarization (I_{tail} current) than at steady-state during the activating step (I_{ss}). The I_{ss}/I_{tail} ratio quantifies I_{Kr} inactivation, a property pivotal in setting I_{Kr} profile during the AP.

RvD1 substantially inhibited I_{Kr} in a concentration-dependent fashion. Thus, for steps to −10 mV, I_{ss} was slightly inhibited by 21.8

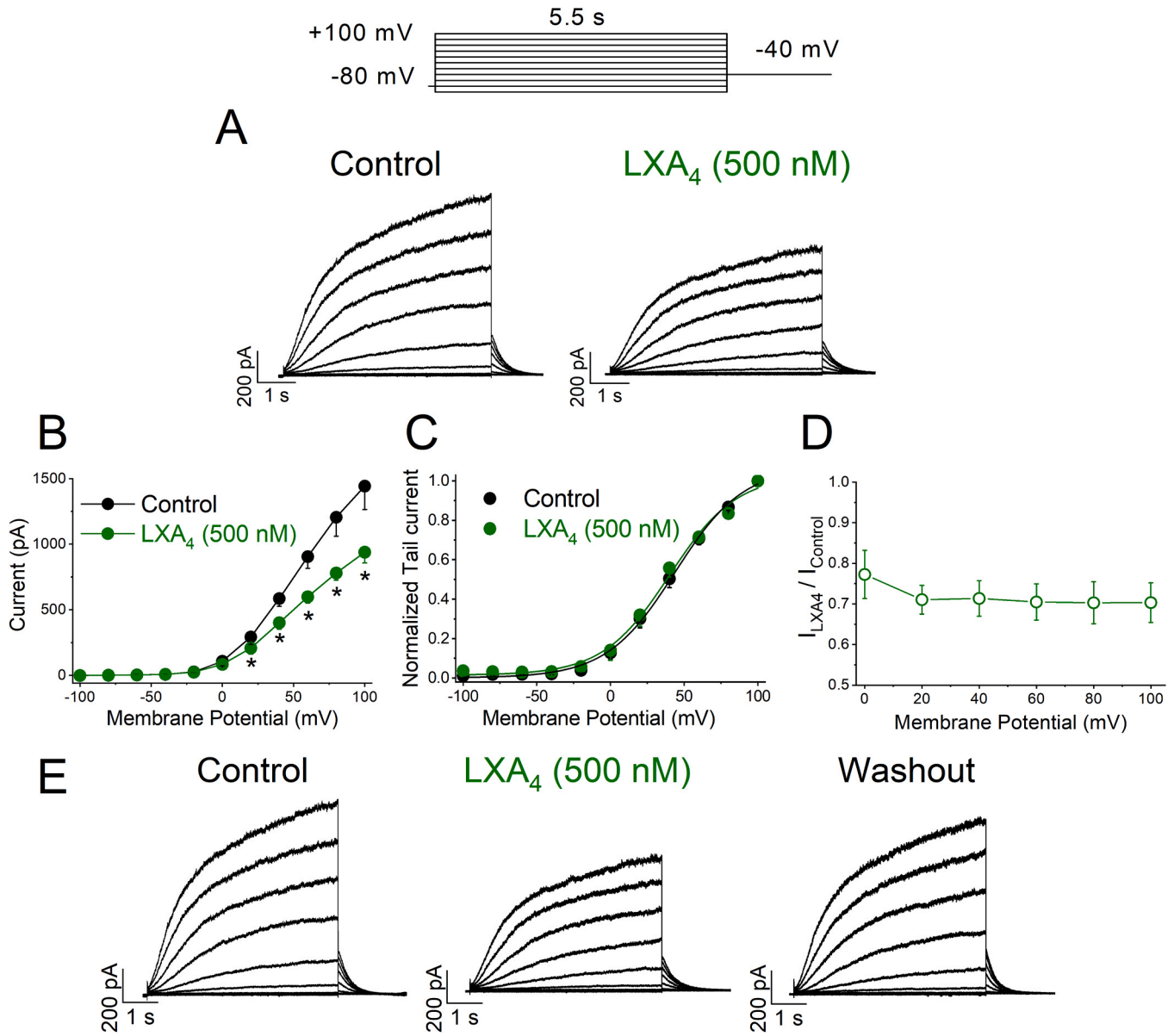

Fig. 2. Voltage-dependent effects of LXA_4 on $K_V7.1/KCNE1$ (I_{Ks}) in transiently transfected COS-7 cells. A: Current traces were obtained after applying the pulse protocol shown in the top, both in the absence and in the presence of LXA_4 (500 nM). B: I-V relationships obtained under control conditions and after perfusion with LXA_4. C: Activation curves of I_{Ks} obtained after plotting the maximum tail current amplitude vs. the previous step potential in the absence and in the presence of LXA_4. D: Ratio between the current in the presence and in the absence of LXA_4. E: Representative traces of LXA_4 wash-out on I_{Ks}. Data are shown as the mean ± SEM. * : $P < 0.05$ (Paired Student's *t*-test), n = 5.

± 5.9 % (n = 4, $P > 0.05$) and 45.3 ± 9.4 % (n = 4, $P > 0.05$) at 5 and 50 nM RvD1, respectively (Figure S4). However, after the same step potential, I_{tail} was inhibited by 31.7 ± 4.6 % (n = 4, $P < 0.05$ vs I_{ss} block) and 56.1 ± 9.5 % (n = 4, $P < 0.05$ vs I_{ss} block) at 5 and 50 nM RvD1, respectively (Fig. 6A-D and S4). Accordingly, RvD1 increased the I_{ss}/I_{tail} significantly (Figure S4). RvD1 100 nM completely blocked I_{Kr} (Figure S6A). The I_{Kr} activation $V_{1/2}$ and slope factor were not modified by 5 nM RvD1 (Table 1, Fig. 6D). However, 50 nM RvD1 negatively shifted the midpoint of the activation curve (-6.2 ± 0.9 mV, P < 0.05), while leaving the slope factor unchanged (Table 1, Fig. 6D).

3.3.4. *RvD1 effects on $K_{ir}2.1$ (COS-7 cells)*

$K_{ir}2.1$ channels belong to the inward-rectifier potassium family and are expressed in excitable and non-excitable cells where they carry I_{K1} [44]. Outward I_{K1} is very small (strong inward rectification), thus steady-state inward I_{K1} was measured to quantify RvD1 effect. RvD1 5 and 50 nM similarly inhibited I_{K1}. For instance, at −120 mV I_{K1} was reduced by 44.6 ± 2.0 % (n = 3, $P < 0.05$) and 46.9 ± 4.4 % (n = 4, $P < 0.05$) by 5 and 50 nM RvD1 respectively, measured at the end of 500 ms pulses. As shown by the I-V relationship, RvD1 blocked inward I_{K1} (at membrane potentialsbetween −140 and −70 mV), whereas outward I_{K1} was, if anything, slighly increased by RvD1 (Fig. 6F). Inward I_{K1} tended to decrease over time during the voltage step, a pattern accentuated by RvD1 (Fig. 6E); this might reflect a slow component of RvD1 interaction with the channel.

Figure S6 summarizes RvD1 effect on the channels analyzed in this study. It plots the percent current inhibition at the activation midpoint for each ion channel.

3.4. *Computational modeling of RvD1 on cardiac AP*

Numerical models were used to predict the effect of RvD1 on

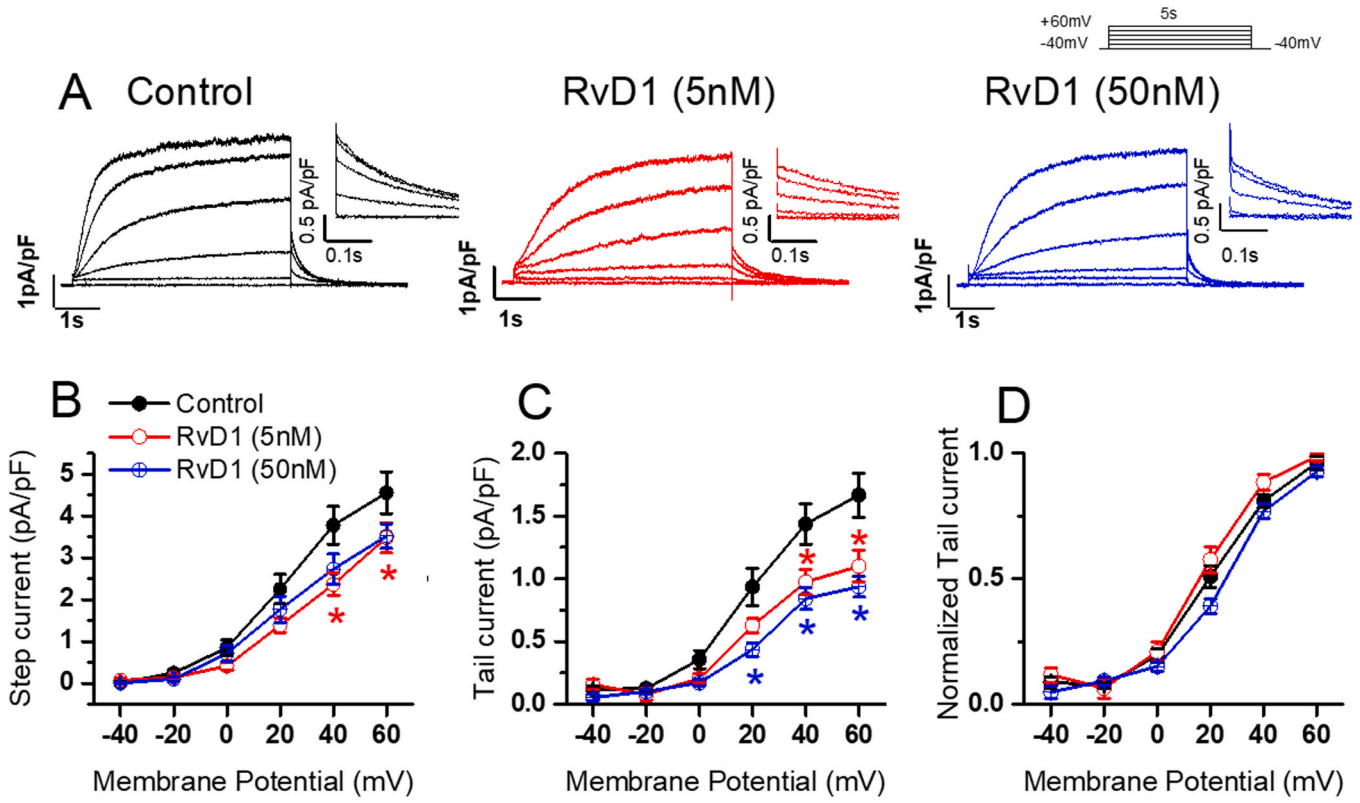

Fig. 3. RvD1 inhibition on I_{Ks} of guinea-pig cardiomyocytes. A: Representative traces of I_{Ks} at various test potential in the 3 groups of myocytes: control (black), RvD1 5 nM (red) and RvD1 50 nM (blue); I_{Ks} tail currents magnified in the insets. B: Average (± SEM) I-V relationships for I_{Ks} at the end of the depolarizing step, C: I_{Ks} "tail current". D: I_{Ks} voltage-dependent activation. n > 6 for all groups, * $P < 0.05$ vs. Control (Two way ANOVA).

ventricular (BPS model for endocardial, epicardial and M cells) and atrial (MBS model) AP morphology (Fig. 7, Tables 4–5).

RvD1 dose-dependently prolonged APD in all types of ventricular myocytes (Fig. 7). In atrial cells, APD prolongation was smaller and substantial only at 50 nM RvD1. In all cases, the main contribution to APD prolongation was given by I_{Kr} inhibition, as suggested by simulations in which only this current was modulated (see Table 4).

To rule out model dependency of the results, the simulations have been performed by using also the established ORd and K models and the AP behaviours are shown in Figure S5 and Tables S1-S2. Results are fully consistent with those obtained with the more recently developed BPS and MBS models. As only remarkable difference, in M cells, the effect of 50 nM of RvD1 was even exacerbated inducing membrane potential bistability and plateau-level oscillations (EADs) in M cells (Figure S5).

4. Discussion

In the current study, we analyzed the effects of two derivatives from n-3 PUFAs and n-6 PUFAs metabolism, RvD1 and LXA_4 on VG cardiac potassium currents. The effect on I_{Ks} was consistent between ventricular myocytes and transfected cell-lines; only the latter were used to test the remaining currents. Our results demonstrate that both SPMs inhibit I_{Ks}, but RvD1 effect was larger than that of LXA_4. Noteworthy, RvD1 blocking effect on I_{Ks} was diminished when only the alpha-subunit of the $K_V7.1$ channel was expressed, thus indicating that KCNE1 is also a target of RvD1. RvD1 also inhibited I_{Kr} ($K_V11.1$ channel) substantially and dose-dependently, producing changes in the current rectifying behavior (the I_{ss}/I_{tail} ratio) of potential relevance for the AP profile.

The potency of the RvD1 to inhibit $K_V1.5$, $K_V4.3$/KChIP2 and Kir2.1 channels was negligible in comparison to that observed on $K_V7.1$/KCNE1 and $K_V11.1$ channels. Finally, we used a holistic approach to predict RvD1 effects on cardiac action potentials by using different computational models. *In silico* results indicate that RvD1 prolongs the ventricular APD in a dose-dependent manner, mainly due to its inhibitory effect on I_{Kr} (Fig. 7, Table 4).

4.1. Differences between experimental models and effect peculiarities

RvD1 and LXA_4 inhibited I_{Ks} both in native guinea-pig myocytes and in a heterologous expression system (COS-7 cells); however, the magnitude of effects differed between the experimental models. Indeed, whereas in myocytes, RvD1 effects on I_{Ks} were relatively small and saturated already at the lower concentration, a greater and dose-dependent effect was observed in COS-7 cells. Nevertheless, at the same concentration (500 nM), LXA_4 effects were larger in myocytes than in COS-7 cells. These discrepancies might reflect: i) a different response to SPMs of human (COS-7 cells) vs guinea-pig channel, ii) dependency of the response on "channelosome" proteins, available in the native myocytes but not in the heterologous system, or iii) that the effects observed in cardiomyocytes might be partially due to the interaction of the SPMs with their membrane receptor (GPR32 or ALX/FPR2). Although the use of a heterologous system might indeed represent a limitation of the present study, this experimental model allows us to study the effect of SPMs on the ion currents in more detail. It has been described that the expression levels of RvD1 and LXA_4 receptors in a given tissue change depending on its degree of inflammation [14]. Moreover, RvD1 changes the expression levels of ion channels in an AF mice model [6]. Also, RvD1 produces potent pro-resolving actions in myocardial infarction-mediated injury [2] and the SPMs receptor FPR2 plays a crucial role in age-related cardiac dysfunction [45]. Hence, heterologous systems provide advantages for studying isolated VG potassium channels, although future studies on ion channels in cardiomyocytes from hypertension, AF, or myocardial infarction animal models would be very interesting to discern the effect of these SPMs on these ion channels

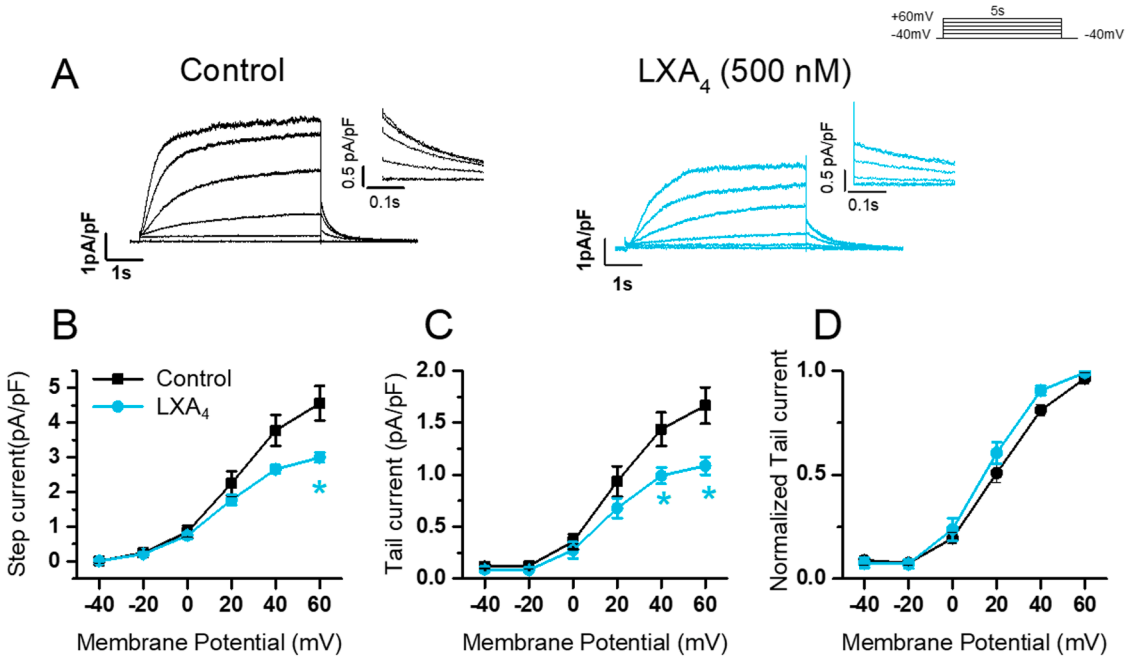

Fig. 4. LXA_4 inhibition on I_{Ks} of guinea-pig cardiomyocytes. Representative traces of I_{Ks} at various test potentials in the 2 groups of myocytes: control (black) and 500 nM (light blue). A: I_{Ks} tail currents magnified in the insets. B: Average (± SEM) I-V relationships for I_{Ks} at the end of the depolarizing step and C: I_{Ks} "tail current" in control and LXA_4 group. D: I_{Ks} voltage-dependent activation in the two experimental groups. Control n > 10, LXA_4 n > 6. * $P < 0.05$ vs. Control (Two way ANOVA).

under certain conditions.

In COS-7 cells transfected with $K_V7.1$ only, RvD1 modified the voltage dependence of I_{Ks} by shifting its activation curve towards positive potentials. This effect was not observed in cells transfected with the whole $K_V7.1$/KCNE1 complex. These results may suggest that, albeit obstructing RvD1 effect on the voltage dependence of $K_V7.1$ gating, KCNE1 potentiates RvD1 inhibitory effect on the alpha channel subunit. It has been reported that most K_V blockers show poor specificity because they mostly bind to conserved residues located in the pore domain (S6) within VG potassium channels [46]. However, KCNE1 regulates $K_V7.1$ conductance by modulating the voltage sensor and its coupling with the pore domain [47,48]. Thus, we speculate that this β-subunit may modulate RvD1 interaction with the channel α-subunit allosterically. The fact that RvD1 also inhibits I_{Kr} current, reinforces our proposal that it binds to the inner pore domain, which represents the most conserved part of these two K_V channels. The observation that RvD1 increased the I_{Ks} step/tail ratio, indicating an effect inversely proportional to the current driving force, suggests that the block may be partially relieved by ions flowing through the channel.

Since RvD1 was more potent than LXA_4 in blocking I_{Ks} in COS-7 cells, we focused on this SPM to analyze its effects on other cardiac K_V channels under heterologous expression. RvD1 effects on I_{Kur}, I_{to} and I_{K1} were considerably smaller than on I_{Ks}. A more substantial inhibitory effect was observed for I_{Kr} and found to be the most significant in prolonging repolarization in numerical simulations. The degree of block of I_{Kr} induced by RvD1 measured at the tail current is greater than that observed in the depolarizing step, which strongly suggest that RvD1 binds to the open state of the channel. The effects on I_{Kr} rectification (I_{ss}/I_{tail} ratio) suggests RvD1 interference with the inactivation gating and might change the impact of I_{Kr} blockade on the AP profile (i.e. reduce the effect on phase 3 as compared to that on phase 2).

4.2. Pathophysiological relevance

RvD1 and LXA_4 are enzymatically synthesized in response to inflammation during the resolution of the inflammation process; indeed, their levels increase during the resolution phase or inflammation [49]. Serum levels of RvD1 of ≅ 160 pg/ml (0.4 nM) have been reported in humans [50]. The present study tested ~10–100-fold higher RvD1 concentrations; therefore the direct pathophysiological relevance of results may be questioned. Nonetheless, in local inflammation, tissue metabolites concentration might exceed by far circulating levels and RvD1 concentration is increased by blood coagulation [51], which is common in AF.

Inflammation has been described as a component of AF-induced atrial remodeling and contributes to atrial cardiomyopathy [5,6]. In an AF mice model, it has been described a dowregulation of the mRNA coding several potassium channels (including $K_V7.1$, $K_V1.5$, $Ca_V1.2$ and $K_{ir}2.1$), whereas $K_V1.3$ was upregulated. Moreover, treatment of these experimental AF mice with RvD1 reverted this mRNA pattern [6]. Notably, the "metabolic syndrome" (encompassing hypertension, insulin resistance and obesity), a known risk factor for arrhythmogenesis, is characterized by a systemic inflammatory state [2,10,14,52]. Recent studies have shown that RvD1 attenuates atrial fibrosis and reduces AF-inducibility, effects associated mainly to reversal of inflammation-induced structural and functional changes [5,6]. Nonetheless, enhancement of potassium currents (e.g. I_{Ks}) has been observed in cardiomyocytes from patients with chronic AF [53] and RvD1 reversed atrial APD shortening in an ischemic heart failure model [5]. Moreover, palmitic acid, another inflammatory lipid, increased I_{Ks} and I_{Kr} density in COS-7 cells and shortened APD in guinea-pig cardiomyocytes [52]. Hence, direct inhibition of cardiac potassium channels, observed in the present work, might contribute to SPMs protective effect against arrhythmias, AF in particular.

A further possibility is that K^+ currents inhibition by SPMs, possibly in immune cells, may contribute to their antiinflammatory action. Indeed, dofetilide a potent I_{Kr} blocker, has been reported to reduce the levels of IL-6, a cytokine involved in atrial inflammation [54]. However, the relationship between inhibition of K^+ currents and IL-production remains uncertain.

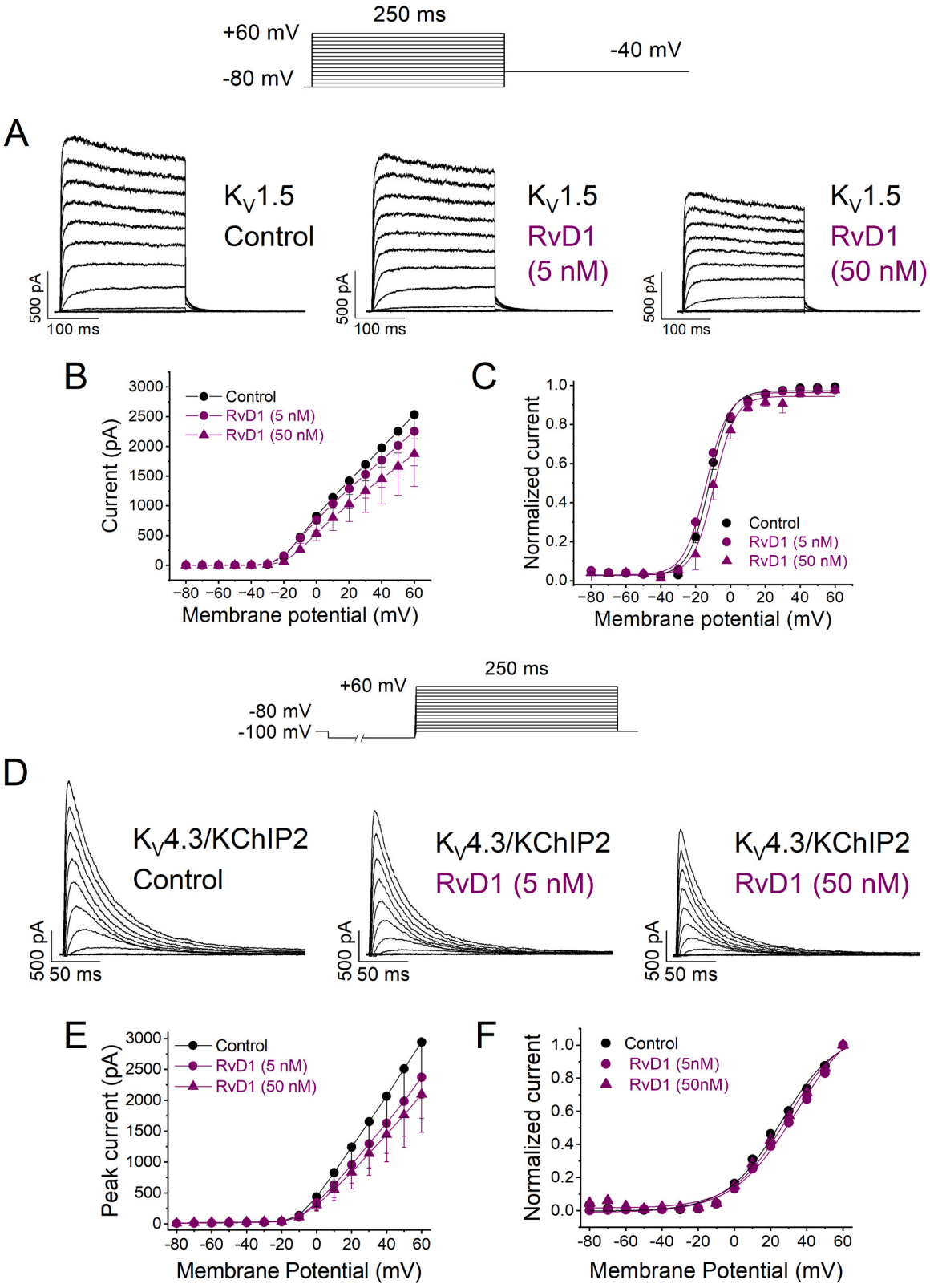

Fig. 5. Effects of RvD1 on $K_V1.5$ (I_{Kur}) and $K_V4.3$/KChIP2 (I_{to}) in stable transfected *Ltk*$^-$ cells and transiently transfected CHO cells, respectively. Currents were elicited after applying the protocol shown on the top of the figure. Representative traces of I_{Kur} (A) and I_{to} (D) currents in *Ltk*$^-$ and CHO cells recorded in the absence (control) and in the presence of 5 and 50 nM RvD1. B: I-V I_{Kur} relationships obtained after plotting the current at the end of 250 ms vs. membrane potential, in the absence and the presence of RvD1. C: Activation curves of I_{Kur} in the absence and the presence of RvD1. E: I-V relationships were obtained after plotting the current measured at the maximum peak for every membrane potential tested vs. membrane potential, in the absence and the presence of RvD1. F: Activation curves of I_{to} in the absence and in the presence of RvD1. Data are shown as the mean ± SEM. * : $P < 0.05$ (Paired Student's *t*-test), n = 4–8 per group.

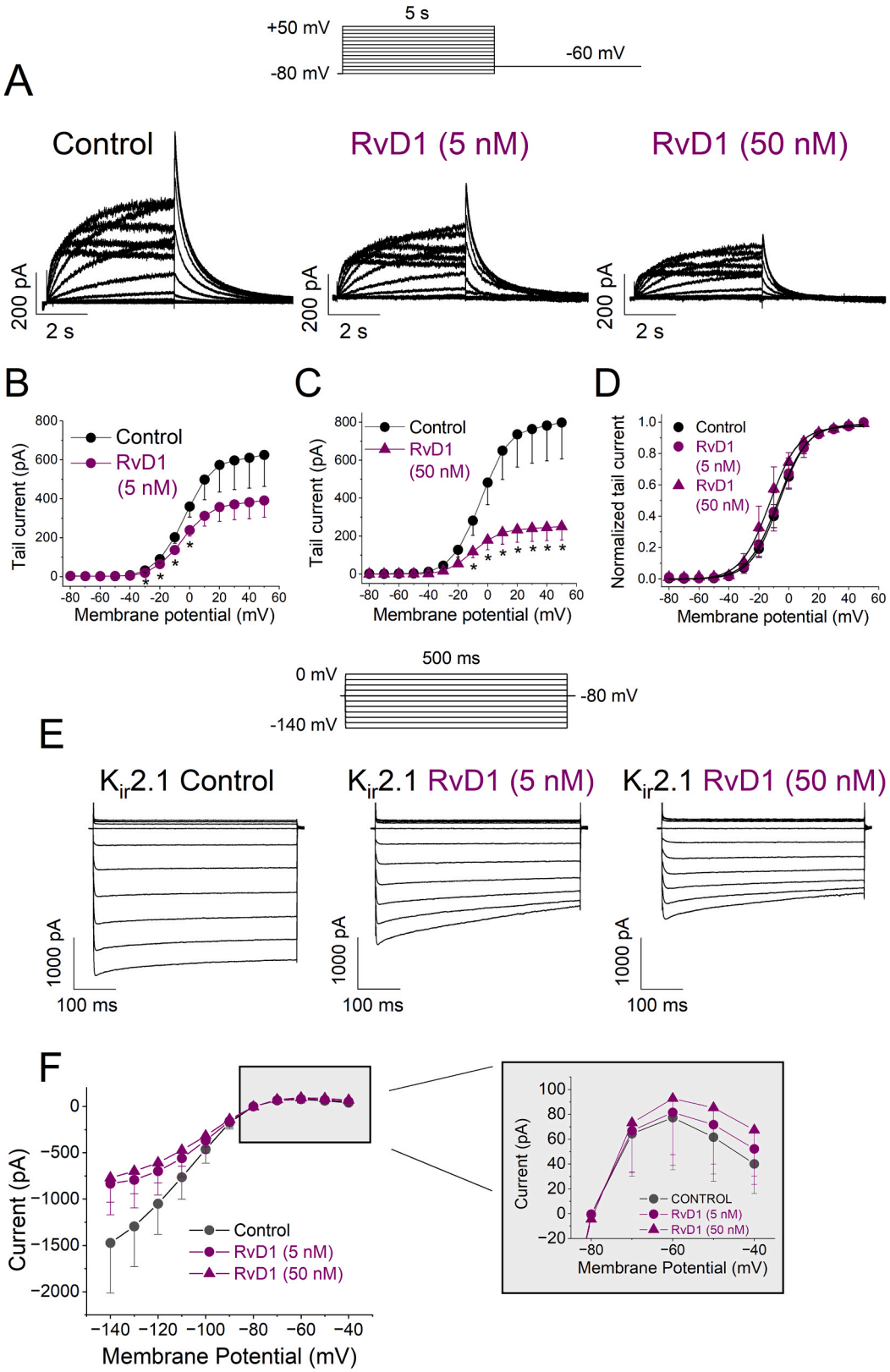

Fig. 6. Effects of RvD1 on $K_V11.1$ (I_{Kr}) and $K_{ir}2.1$ (I_{K1}) in transiently transfected COS-7 cells. Currents were elicited after applying the protocol shown on the top of the figure (for I_{Kr} (A) and on top of original traces (for I_{K1}, E). A: Representative traces of I_{Kr} recorded in the absence (control) and in the presence of 5 and 50 nM RvD1. B and C: I_{Kr} tail currents plotted vs. membrane potentials tested, in the absence and the presence of 5 nM RvD1 and 50 nM RvD1. D: Activation curves of I_{Kr} in the absence and the presence of RvD1. E: Representative traces of I_{K1} recorded in the absence (control) and in the presence of 5 and 50 nM RvD1. F: I-V relationships obtained after plotting the current at the end of 500 ms vs. membrane potential, in the absence and the presence of RvD1. The inset shows RvD1 effect on I_{K1} measured between −80 mV and −40 mV of the membrane potential. Data are shown as the mean ± SEM. * : $P < 0.05$ (Paired Student's *t*-test), n = 4–5 per group.

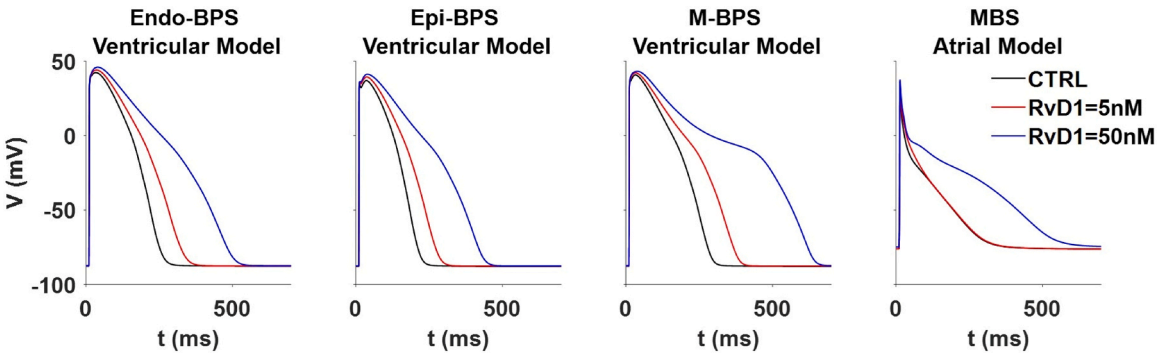

Fig. 7. Computational modeling of RvD1 on cardiac AP. BPS ventricular cell computer model was used to examine the effects of RvD1, on AP morphology in A: endocardial, B: epicardial, and C: M cells. D: MBS human atrial AP model was used to examine the effects of RvD1, on atrial AP morphology.

Table 4
Computational modeling APD_{90} results with the BPS model.

	APD_{90} (ms)			Δ%		
	Endo	*Epi*	*M*	*Δ% Endo*	*Δ% Epi*	Δ% M
CTRL	238	200	267			
RvD1 (5 nM)	310	259	354	30	30	33
RvD1 (5 nM) only I_{Ks}	248	207	281	4	4	5
RvD1 (5 nM) only I_{to}	249	209	282	5	5	6
RvD1 (5 nM) only I_{Kr}	311	260	356	31	30	33
RvD1 (50 nM)	467	405	604	96	103	126
RvD1 (50 nM) only I_{Ks}	257	213	294	8	7	10
RvD1 (50 nM) only I_{to}	249	209	282	5	5	6
RvD1 (50 nM) only I_{Kr}	425	362	505	79	81	89

Table 5
Computational modeling APD results with the atrial MBS model.

	APD (ms)	Δ%
CTRL	249	
RvD1 (5 nM)	253	2
RvD1 (5 nM) only I_{Ks}	258	3.6
RvD1 (5 nM) only I_{to}	265	6.4
RvD1 (5 nM) only I_{Kr}	259	4
RvD1 (5 nM) only I_{Kur}	223	−10
RvD1 (50 nM)	478	92
RvD1 (50 nM) only I_{Ks}	264	6
RvD1 (50 nM) only I_{to}	263	5.6
RvD1 (50 nM) only I_{Kr}	270	8.4
RvD1 (50 nM) only I_{Kur}	328	31.7

Using computational modeling, we examined the expected impact of RvD1 on atrial and ventricular repolarization. The results of these studies confirm that RvD1 effect on K^+ currents may substantially prolong repolarization in both tissues. Albeit potentially beneficial in conditions in which shortened repolarization may contribute to arrhythmogenesis (e.g. AF), this effect might instead be of concern when ventricular repolarization is primarily prolonged, or repolarization reserve is reduced [5]. The present results may thus be relevant to the design and use of SPMs-based agents, as part of the Comprehensive in Vitro Proarrhythmia Assay (CiPA) initiative [55].

5. Conclusions

RvD1 inhibits several K^+ currents relevant for myocardial repolarization. Since RvD1 levels change in different cardiovascular pathologies, these results are pathophysiologically relevant. It should be noted that inhibition of K^+ current may be beneficial in some conditions and undesirable in others.

CRediT authorship contribution statement

de la Cruz Alicia: Writing – original draft, Methodology, Investigation, Formal analysis, Conceptualization. **Valenzuela Carmen:** Writing – review & editing, Supervision, Project administration, Funding acquisition, Formal analysis, Conceptualization. **Severi Stefano:** Supervision, Methodology, Investigation, Funding acquisition, Formal analysis. **Zaza Antonio:** Writing – review & editing, Methodology, Investigation, Formal analysis. **Ronchi Carlotta:** Methodology, Investigation, Formal analysis. **Bartolucci Chiara:** Methodology, Investigation, Formal analysis. **Socuéllamos Paula:** Methodology, Investigation, Formal analysis. **de Benito-Bueno Angela:** Methodology, Investigation, Formal analysis.

Statement of ethical approval

All animal care and experimental procedures were performed conforming to the NIH guidelines (Guide for the care and use of laboratory animals) revised in 2011; and from Directive 2010/63/EU of the European Parliament on the protection of animals used for scientific purposes and approved by the University of Milano-Bicocca ethics review board.

Funding

This publication is the results of the: Grants PID2019–104366RB-C21 (to C.V.), PID2022–137214OB-C21 (to C.V.); funded by MCIN/AEI/10.13039/501100011033; Grant CB/11/00222 funded by Instituto de Salud Carlos III CIBERCV (to C.V.); Grants BES-2017–080184 (to A.d.B.-B.); Grant FPU17/02731 (to P.G.S.) funded by Ministerio de Ciencia e Innovación. NextGenerationEU through the Italian Ministry of University (C.B. and S.S) and Research under PNRR - M4C2-I1.3 Project PR 00000019 "HEAL ITALIA" (to S.S). CUP J33C22002920006 (C.B. and S. S).

Conflict of interest

The authors declare that they have no known competing financial interests or personal relationships that could have appeared to influence the work reported in this paper.

Declaration of Competing Interest

none. Authors do not have nothing to declare.

Acknowledgments

The authors are grateful to Dr Eva Delpón of the Universidad Complutense de Madrid, Spain for kindly providing us with $K_{ir}2.1$ cloned into pcDNA3.1, to Drs S. Nattel, T. E. Hébert, and W. Weerapura of the

Université de Montréal, Canada for kindly providing us with K_V11.1 cloned into pcDNA3.1 and to Dr Michael M. Tamkun for providing us the stable cell line expressing K_V1.5 channels. We also thank Dr. Lisardo Boscá for his helpful comments.

Appendix A. Supporting information

Supplementary data associated with this article can be found in the online version at doi:10.1016/j.biopha.2025.118083.

Data Availability

Data will be made available on request.

References

[1] X. Liu, X. Wang, X. Duan, D. Poorun, J. Xu, S. Zhang, L. Gan, M. He, K. Zhu, Z. Ming, F. Hu, H. Chen, Lipoxin A4 and its analog suppress inflammation by modulating HMGB1 translocation and expression in psoriasis, Sci. Rep. 7 (1) (2017) 7100, https://doi.org/10.1038/s41598-017-07485-1.

[2] V. Kain, K.A. Ingle, R.A. Colas, J. Dalli, S.D. Prabhu, C.N. Serhan, M. Joshi, G. V. Halade, Resolvin D1 activates the inflammation resolving response at splenic and ventricular site following myocardial infarction leading to improved ventricular function, J. Mol. Cell Cardiol. 84 (2015) 24–35, https://doi.org/10.1016/j.yjmcc.2015.04.003.

[3] B.D. Levy, C.B. Clish, B. Schmidt, K. Gronert, C.N. Serhan, Lipid mediator class switching during acute inflammation: signals in resolution, Nat. Immunol. 2 (7) (2001) 612–619, https://doi.org/10.1038/89759.

[4] C.N. Serhan, Novel omega – 3-derived local mediators in anti-inflammation and resolution, Pharm. Ther. 105 (1) (2005) 7–21, https://doi.org/10.1016/j.pharmthera.2004.09.002.

[5] R. Hiram, F. Xiong, P. Naud, J. Xiao, D.K. Sosnowski, E. Le Quilliec, A. Saljic, I. H. Abu-Taha, M. Kamler, C.A. LeBlanc, D.G.F. Al-U'Datt, M.G. Sirois, T.E. Hebert, J.F. Tanguay, J.C. Tardif, D. Dobrev, S. Nattel, An inflammation resolution-promoting intervention prevents atrial fibrillation caused by left ventricular dysfunction, Cardiovasc Res 120 (4) (2024) 345–359, https://doi.org/10.1093/cvr/cvad175.

[6] R. Hiram, F. Xiong, P. Naud, J. Xiao, M. Sirois, J.F. Tanguay, J.C. Tardif, S. Nattel, The inflammation-resolution promoting molecule resolvin-D1 prevents atrial proarrhythmic remodelling in experimental right heart disease, Cardiovasc Res 117 (7) (2021) 1776–1789, https://doi.org/10.1093/cvr/cvaa186.

[7] M. Wang, W. Pan, C. Wei, J. Liu, J. Zhang, J. Yu, M. Zhao, S. Xu, J. Ye, Z. Wang, D. Ye, Y. Feng, Y. Xu, J. Wan, The Anti-Inflammatory Mediator 17(R)-Resolvin D1 Attenuates Pressure Overload-Induced Cardiac Hypertrophy and Fibrosis, Drug Des. Devel Ther. 17 (2023) 3073–3083, https://doi.org/10.2147/DDDT.S421894.

[8] M. Wang, M. Liu, J. Zhang, J. Liu, J. Ye, Y. Xu, Z. Wang, D. Ye, M. Zhao, J. Wan, Resolvin D1 protects against sepsis-induced cardiac injury in mice, Biofactors 46 (5) (2020) 766–776, https://doi.org/10.1002/biof.1668.

[9] M. Wang, J. Zhang, M. Zhao, J. Liu, J. Ye, Y. Xu, Z. Wang, D. Ye, D. Li, J. Wan, Resolvin D1 Attenuates Doxorubicin-Induced Cardiotoxicity by Inhibiting Inflammation, Oxidative and Endoplasmic Reticulum Stress, Front Pharm. 12 (2021) 749899, https://doi.org/10.3389/fphar.2021.749899.

[10] G.V. Halade, V. Kain, C.N. Serhan, Immune responsive resolvin D1 programs myocardial infarction-induced cardiorenal syndrome in heart failure, FASEB J. 32 (7) (2018) 3717–3729, https://doi.org/10.1096/fj.201701173RR.

[11] J.S. Duffield, S. Hong, V.S. Vaidya, Y. Lu, G. Fredman, C.N. Serhan, J.V. Bonventre, Resolvin D series and protectin D1 mitigate acute kidney injury, J. Immunol. 177 (9) (2006) 5902–5911, https://doi.org/10.4049/jimmunol.177.9.5902.

[12] J.F. Lima-Garcia, R.C. Dutra, K. da Silva, E.M. Motta, M.M. Campos, J.B. Calixto, The precursor of resolvin D series and aspirin-triggered resolvin D1 display anti-hyperalgesic properties in adjuvant-induced arthritis in rats, Br. J. Pharm. 164 (2) (2011) 278–293, https://doi.org/10.1111/j.1476-5381.2011.01345.x.

[13] N.G. Bazan, J.M. Calandria, C.N. Serhan, Rescue and repair during photoreceptor cell renewal mediated by docosahexaenoic acid-derived neuroprotectin D1, J. Lipid Res 51 (8) (2010) 2018–2031, https://doi.org/10.1194/jlr.R001131.

[14] L.S. Diaz Del Campo, A.B. Garcia-Redondo, C. Rodriguez, C. Zaragoza, S. Duro-Sanchez, F. Palmas, A. de Benito-Bueno, P.G. Socuellamos, D.A. Peraza, R. Rodrigues-Diez, C. Valenzuela, J. Dalli, M. Salaices, A.M. Briones, Resolvin D2 attenuates cardiovascular damage in angiotensin II-induced hypertension, Hypertension 80 (1) (2023) 84–96, https://doi.org/10.1161/HYPERTENSIONAHA.122.19448.

[15] S. Bang, S. Yoo, T.J. Yang, H. Cho, S.W. Hwang, 17(R)-resolvin D1 specifically inhibits transient receptor potential ion channel vanilloid 3 leading to peripheral antinociception, Br. J. Pharm. 165 (3) (2012) 683–692, https://doi.org/10.1111/j.1476-5381.2011.01568.x.

[16] C. Moreno, P. Prieto, A. Macias, M. Pimentel-Santillana, A. de la Cruz, P.G. Traves, L. Bosca, C. Valenzuela, Modulation of voltage-dependent and inward rectifier potassium channels by 15-epi-lipoxin-A4 in activated murine macrophages: implications in innate immunity, J. Immunol. 191 (12) (2013) 6136–6146, https://doi.org/10.4049/jimmunol.1300235.

[17] H.J. Pyo, X. An, H. Cho, The role of free fatty acid receptor pathways in a selective regulation of TRPA1 and TRPV1 by resolvins in primary sensory neurons, J. Cell Physiol. 237 (9) (2022) 3651–3660, https://doi.org/10.1002/jcp.30826.

[18] B.M. Bohannon, X. Wu, X. Wu, M.E. Perez, S.I. Liin, H.P. Larsson, Polyunsaturated fatty acids produce a range of activators for heterogeneous IKs channel dysfunction, J. Gen. Physiol. 152 (2) (2020), https://doi.org/10.1085/jgp.201912396.

[19] B.M. Bohannon, M.E. Perez, S.I. Liin, H.P. Larsson, omega-6 and omega-9 polyunsaturated fatty acids with double bonds near the carboxyl head have the highest affinity and largest effects on the cardiac I(K)(s) potassium channel, Acta Physiol. (Oxf.) 225 (2) (2019) e13186, https://doi.org/10.1111/apha.13186.

[20] C. Moreno, A. de la Cruz, A. Oliveras, S.R. Kharche, M. Guizy, N. Comes, T. Stary, C. Ronchi, M. Rocchetti, I. Baro, G. Loussouarn, A. Zaza, S. Severi, A. Felipe, C. Valenzuela, Marine n-3 PUFAs modulate IKs gating, channel expression, and location in membrane microdomains, Cardiovasc Res 105 (2) (2015) 223–232, https://doi.org/10.1093/cvr/cvu250.

[21] M. Guizy, C. Arias, M. David, T. Gonzalez, C. Valenzuela, Omega-3 and omega-6 polyunsaturated fatty acids block HERG channels, Am. J. Physiol. Cell Physiol. 289 (5) (2005) C1251–C1260, https://doi.org/10.1152/ajpcell.00036.2005.

[22] Y.F. Xiao, J.X. Kang, J.P. Morgan, A. Leaf, Blocking effects of polyunsaturated fatty acids on Na+ channels of neonatal rat ventricular myocytes, Proc. Natl. Acad. Sci. USA 92 (24) (1995) 11000–11004, https://doi.org/10.1073/pnas.92.24.11000.

[23] Y.F. Xiao, A.M. Gomez, J.P. Morgan, W.J. Lederer, A. Leaf, Suppression of voltage-gated L-type Ca2+ currents by polyunsaturated fatty acids in adult and neonatal rat ventricular myocytes, Proc. Natl. Acad. Sci. USA 94 (8) (1997) 4182–4187, https://doi.org/10.1073/pnas.94.8.4182.

[24] S.I. Liin, J.E. Larsson, R. Barro-Soria, B.H. Bentzen, H.P. Larsson, Fatty acid analogue N-arachidonoyl taurine restores function of I(Ks) channels with diverse long QT mutations, Elife 5 (2016), https://doi.org/10.7554/eLife.20272.

[25] C. Valenzuela, M-channels and n-3 polyunsaturated fatty acids: role in pain and epilepsy, Acta Physiol. (Oxf.) 218 (1) (2016) 7–9, https://doi.org/10.1111/apha.12734.

[26] A. Zaza, M. Rocchetti, A. Brioschi, A. Cantadori, A. Ferroni, Dynamic Ca2+ -induced inward rectification of K+ current during the ventricular action potential, Circ. Res 82 (9) (1998) 947–956, https://doi.org/10.1161/01.res.82.9.947.

[27] M. Longobardo, E. Delpon, R. Caballero, J. Tamargo, C. Valenzuela, Structural determinants of potency and stereoselective block of hKv1.5 channels induced by local anesthetics, Mol. Pharm. 54 (1) (1998) 162–169, https://doi.org/10.1124/mol.54.1.162.

[28] B. Jiang, X. Sun, K. Cao, R. Wang, Endogenous Kv channels in human embryonic kidney (HEK-293) cells, Mol. Cell Biochem 238 (1-2) (2002) 69–79, https://doi.org/10.1023/a:1019907104763.

[29] D.J. Snyders, M.M. Tamkun, P.B. Bennett, A rapidly activating and slowly inactivating potassium channel cloned from human heart. Functional analysis after stable mammalian cell culture expression, J. Gen. Physiol. 101 (4) (1993) 513–543, https://doi.org/10.1085/jgp.101.4.513.

[30] L. Franqueza, C. Valenzuela, J. Eck, M.M. Tamkun, J. Tamargo, D.J. Snyders, Functional expression of an inactivating potassium channel (Kv4.3) in a mammalian cell line, Cardiovasc Res 41 (1) (1999) 212–219, https://doi.org/10.1016/s0008-6363(98)00220-x.

[31] M. David, A. Macias, C. Moreno, A. Prieto, R. Martinez-Marmol, R. Vicente, T. Gonzalez, A. Felipe, M.M. Tamkun, C. Valenzuela, Protein kinase C (PKC) activity regulates functional effects of Kvbeta1.3 subunit on KV1.5 channels: identification of a cardiac Kv1.5 channelosome, J. Biol. Chem. 287 (25) (2012) 21416–21428, https://doi.org/10.1074/jbc.M111.328278.

[32] D.A. Peraza, P. Cercos, P. Miaja, Y.G. Merinero, L. Lagartera, P.G. Socuellamos, C. Izquierdo Garcia, S.A. Sanchez, A. Lopez-Hurtado, M. Martin-Martinez, L. A. Olivos-Ore, J.R. Naranjo, A.R. Artalejo, M. Gutierrez-Rodriguez, C. Valenzuela, Identification of IQM-266, a novel DREAM ligand that modulates K(V)4 currents, Front Mol. Neurosci. 12 (2019) 11, https://doi.org/10.3389/fnmol.2019.00011.

[33] C. Arias, T. Gonzalez, I. Moreno, R. Caballero, E. Delpon, J. Tamargo, C. Valenzuela, Effects of propafenone and its main metabolite, 5-hydroxypropafenone, on HERG channels, Cardiovasc Res 57 (3) (2003) 660–669, https://doi.org/10.1016/s0008-6363(02)00726-5.

[34] A. Oliveras, M. Roura-Ferrer, L. Sole, A. de la Cruz, A. Prieto, A. Etxebarria, J. Manils, D. Morales-Cano, E. Condom, C. Soler, A. Cogolludo, C. Valenzuela, A. Villarroel, N. Comes, A. Felipe, Functional assembly of Kv7.1/Kv7.5 channels with emerging properties on vascular muscle physiology, Arterioscler. Thromb. Vasc. Biol. 34 (7) (2014) 1522–1530, https://doi.org/10.1161/ATVBAHA.114.303801.

[35] C. Arias, M. Guizy, M. David, S. Marzian, T. Gonzalez, N. Decher, C. Valenzuela, Kvbeta1.3 reduces the degree of stereoselective bupivacaine block of Kv1.5 channels, Anesthesiology 107 (4) (2007) 641–651, https://doi.org/10.1097/01.anes.0000282100.32923.5c.

[36] L. Franqueza, M. Longobardo, J. Vicente, E. Delpon, M.M. Tamkun, J. Tamargo, D. J. Snyders, C. Valenzuela, Molecular determinants of stereoselective bupivacaine block of hKv1.5 channels, Circ. Res. 81 (6) (1997) 1053–1064, https://doi.org/10.1161/01.res.81.6.1053.

[37] C. Bartolucci, E. Passini, J. Hyttinen, M. Paci, S. Severi, Simulation of the effects of extracellular calcium changes leads to a novel computational model of human ventricular action potential with a revised calcium handling, Front Physiol. 11 (2020) 314, https://doi.org/10.3389/fphys.2020.00314.

[38] T. O'Hara, L. Virag, A. Varro, Y. Rudy, Simulation of the undiseased human cardiac ventricular action potential: model formulation and experimental validation, PLoS Comput. Biol. 7 (5) (2011) e1002061, https://doi.org/10.1371/journal.pcbi.1002061.

[39] F. Mazhar, C. Bartolucci, F. Regazzoni, M. Paci, L. Dede, A. Quarteroni, C. Corsi, S. Severi, A detailed mathematical model of the human atrial cardiomyocyte: integration of electrophysiology and cardiomechanics, J. Physiol. 602 (18) (2024) 4543–4583, https://doi.org/10.1113/JP283974.
[40] J.T. Koivumaki, G. Seemann, M.M. Maleckar, P. Tavi, In silico screening of the key cellular remodeling targets in chronic atrial fibrillation, PLoS Comput. Biol. 10 (5) (2014) e1003620, https://doi.org/10.1371/journal.pcbi.1003620.
[41] H. Yucel, A.T. Ozdemir, Low LXA4, RvD1 and RvE1 levels may be an indicator of the development of hypertension, Prostaglandins Leukot. Ess. Fat. Acids 174 (2021) 102365, https://doi.org/10.1016/j.plefa.2021.102365.
[42] O. Karayigit, S.G. Nurkoc, F. Basyigit, E. Kiziltunc, The role of serum resolvin D1 levels in determining the presence and prognosis of ST-SEgment Elevation Myocardial Infarction, Med Princ. Pr. 31 (6) (2022) 548–554, https://doi.org/10.1159/000527064.
[43] V. Chiurchiu, A. Leuti, S. Saracini, D. Fontana, P. Finamore, R. Giua, L. Padovini, R. A. Incalzi, M. Maccarrone, Resolution of inflammation is altered in chronic heart failure and entails a dysfunctional responsiveness of T lymphocytes, FASEB J. 33 (1) (2019) 909–916, https://doi.org/10.1096/fj.201801017R.
[44] D.A. Peraza, A. Povo-Retana, M. Mojena, A.B. Garcia-Redondo, P. Aviles, L. Bosca, C. Valenzuela, Trabectedin modulates macrophage polarization in the tumor-microenvironment. Role of K(V)1.3 and K(V)1.5 channels, Biomed. Pharm. 161 (2023) 114548, https://doi.org/10.1016/j.biopha.2023.114548.
[45] B. Tourki, V. Kain, A.B. Pullen, P.C. Norris, N. Patel, P. Arora, X. Leroy, C. N. Serhan, G.V. Halade, Lack of resolution sensor drives age-related cardiometabolic and cardiorenal defects and impedes inflammation-resolution in heart failure, Mol. Metab. 31 (2020) 138–149, https://doi.org/10.1016/j.molmet.2019.10.008.
[46] E. Wrobel, I. Rothenberg, C. Krisp, F. Hundt, B. Fraenzel, K. Eckey, J.T. Linders, D. J. Gallacher, R. Towart, L. Pott, M. Pusch, T. Yang, D.M. Roden, H.T. Kurata, E. Schulze-Bahr, N. Strutz-Seebohm, D. Wolters, G. Seebohm, KCNE1 induces fenestration in the Kv7.1/KCNE1 channel complex that allows for highly specific pharmacological targeting, Nat. Commun. 7 (2016) 12795, https://doi.org/10.1038/ncomms12795.
[47] G. Kuenze, C.G. Vanoye, R.R. Desai, S. Adusumilli, K.R. Brewer, H. Woods, E. F. McDonald, C.R. Sanders, A.L. George Jr., J. Meiler, Allosteric mechanism for KCNE1 modulation of KCNQ1 potassium channel activation, Elife 9 (2020), https://doi.org/10.7554/eLife.57680.
[48] X. Wu, M.E. Perez, S.Y. Noskov, H.P. Larsson, A general mechanism of KCNE1 modulation of KCNQ1 channels involving non-canonical VSD-PD coupling, Commun. Biol. 4 (1) (2021) 887, https://doi.org/10.1038/s42003-021-02418-1.
[49] C.N. Serhan, B.D. Levy, Resolvins in inflammation: emergence of the pro-resolving superfamily of mediators, J. Clin. Invest 128 (7) (2018) 2657–2669, https://doi.org/10.1172/JCI97943.
[50] A. Croasdell, T.H. Thatcher, R.M. Kottmann, R.A. Colas, J. Dalli, C.N. Serhan, P. J. Sime, R.P. Phipps, Resolvins attenuate inflammation and promote resolution in cigarette smoke-exposed human macrophages, Am. J. Physiol. Lung Cell Mol. Physiol. 309 (8) (2015) L888–L901, https://doi.org/10.1152/ajplung.00125.2015.
[51] P.C. Norris, S. Libreros, N. Chiang, C.N. Serhan, A cluster of immunoresolvents links coagulation to innate host defense in human blood, Sci. Signal 10 (490) (2017), https://doi.org/10.1126/scisignal.aan1471.
[52] A.S. Aromolaran, H.M. Colecraft, M. Boutjdir, High-fat diet-dependent modulation of the delayed rectifier K(+) current in adult guinea pig atrial myocytes, Biochem Biophys. Res. Commun. 474 (3) (2016) 554–559, https://doi.org/10.1016/j.bbrc.2016.04.113.
[53] R. Caballero, M.G. de la Fuente, R. Gomez, A. Barana, I. Amoros, P. Dolz-Gaiton, L. Osuna, J. Almendral, F. Atienza, F. Fernandez-Aviles, A. Pita, J. Rodriguez-Roda, A. Pinto, J. Tamargo, E. Delpon, In humans, chronic atrial fibrillation decreases the transient outward current and ultrarapid component of the delayed rectifier current differentially on each atria and increases the slow component of the delayed rectifier current in both, J. Am. Coll. Cardiol. 55 (21) (2010) 2346–2354, https://doi.org/10.1016/j.jacc.2010.02.028.
[54] C. Hunter, T.B. Kadakia, D. Cooper, M. Perretti, R.C. Schwartz, S.B. Brown, Selective inhibitors of Kv11.1 regulate IL-6 expression by macrophages in response to TLR/IL-1R ligands, ScientificWorldJournal 10 (2010) 1580–1596, https://doi.org/10.1100/tsw.2010.155.
[55] T. Colatsky, B. Fermini, G. Gintant, J.B. Pierson, P. Sager, Y. Sekino, D.G. Strauss, N. Stockbridge, The comprehensive in vitro proarrhythmia assay (CiPA) initiative - Update on progress, J. Pharm. Toxicol. Methods 81 (2016) 15–20, https://doi.org/10.1016/j.vascn.2016.06.002.